Geography and human relationships, vol7, no1, summer 2024, pp:1-17

Modeling Land Surface Temperature and Estimating Methods in Predicting LSD by Remote Sensing Technique in Tabriz County, Iran

Bromand Salahi[*1], Zahra Abdi[2], Mahnaz Saber[3]

1- Ph.D. of climatology, Professor, Department of Physical Geography, University of Mohaghegh Ardabili, Ardabil, Iran.
E-mail: bromand416@yahoo.com
http://orcid.org/0000-0003-4826-6185
2-Ph.D. Student of Climatology, University of Mohaghegh Ardabili, Ardabil, Iran.
3-Ph.D. of Climatology, Department of Physical Geography, Faculty of Social Sciences, University of Mohaghegh Ardabili, Ardabil, Iran
mahnaz.saber@yahoo.com E-mail:

Submit date: 2020/12/09 accept date: 2020/09/03

Abstract

Today, global warming, increasing the Land Surface Temperature, especially in big cities, is one of the environmental problems. The purpose of this article is to estimate the ability of Sebal, improved single-channel and Split window algorithms in estimating Land Surface Temperature on Landsat 8 image data in July 2019 and extracting Land Use maps in 7 classes for Tabriz County using an object-oriented classification method. Matching the temperature maps obtained by using these three mentioned algorithms with the Land Use map and comparing the algorithms with each other in terms of the proximity of their temperature to the Tabriz station is another goal of this article. To estimate the accuracy of the measured temperature, the data of the measured temperature of the Tabriz station at two centimeters above the land (as a representative of Tabriz County) has been used. The results of Sebal, improved single-channel, and Split window algorithms showed the highest temperature for dry pasture use and the lowest temperature for vegetation use, which indicates the importance of vegetation cover in the temperature changes of the studied area. A comparison of the studied algorithms with the temperature measured in the Tabriz station and their adaptation to different uses showed that the improved single-channel algorithm is more consistent with the actual temperature of the actual Land Surface Temperature in Tabriz County. The results of this study can help environmental planners concerned about the increase in air temperature in cities to make more appropriate decisions regarding the control of this phenomenon.

Keywords: Land Surface Temperature, Land Use, Object-Oriented Classification, Tabriz County.

doi: **10.22034/GAHR.2023.416025.1940** ESSN: 2645-3851

Introduction

The rapid growth of cities in developing countries has caused ecological changes on a regional and global scale (Babalola and Akinsanola, 2016). Land Surface Temperature is an essential indicator in studying energy balance models on the Earth's surface and interactions between the Earth and the atmosphere on a regional and global scale (Asghari Saraskanroud et al., 2019). The Land Surface Temperature is the radiant temperature of the surface, and due to the heterogeneity of the surfaces, it shows many spatial changes (Wang and Prigent, 2020). Land Surface Temperature is one of the input data sources for modeling earth surface processes such as actual evapotranspiration, potential evapotranspiration, and net radiation, which are considered important components in environmental studies (Cristóbal et al., 2018). Remote sensing technology is an essential tool for observing the earth using different sensors, and compared to conventional methods, it provides the possibility of conducting large-scale, cheap, and accurate studies.

Thermal remote sensing is a branch of remote sensing science that deals with receiving, processing, and interpreting the data obtained from the electromagnetic spectrum (Sekertekin and Bonafoni, 2020). This remote sensing branch is very important due to the limitation of meteorological stations and the impossibility of measuring temperature in different geographical areas (Asghari Saraskanroud et al., 2019). Sensors in the thermal infrared range receive the Land Surface Temperature, store it in the form of digital images and send it to the earth. These sensors use the active atmospheric window area for better performance. In thermal remote sensing, the atmosphere's temperature is recorded by the sensor, which is very different from the actual Land Surface Temperature, because this radiant temperature is absorbed and diffused by the atmosphere before it reaches the sensor. In the last few decades, various algorithms have been presented to estimate the real Land Surface Temperature using different sensors, and the basis of these algorithms is based on various assumptions of radiation equations.

Atmospheric effects and emissivity are essential factors in calculating surface temperature (Sekertekin and Bonafoni, 2019). Researches shows that urban places are hotter than the surrounding rural areas and in general, this phenomenon is called urban heat island (Valizadeh Kamran et al., 2017). The heat emitted from urban structures plays the most important role in urban heating, especially the heat island of the city, and it is necessary to seriously consider ways to reduce the heat island of the city. Cristóbal et al., (2018) used a single-channel method to retrieve Land Surface Temperature. Using multi-spectral and multi-temporal satellite data, Ang et al., (2018) evaluated the impact of Land Use and land cover changes on Land Surface Temperature in Kuala Lumpur. They showed that the decrease in vegetation cover increases the Land Surface Temperature. Asghari Saraskanroud et al., (2019) monitored the Land Surface Temperature and investigated the Land Use relationship in Ardabil City using Landsat 8 satellite images and a separate window algorithm. They showed that the urban areas with little vegetation have a higher temperature than the areas under agriculture and pastures because the vegetation acts as a barrier to the entry of heat and has an inverse relationship with the surface temperature. Variations of urban heat island (UHI) intensity in Istanbul using meteorological data measured at six stations were analyzed by Ünal et al., (2020).

Naseri (2020) used a single-channel algorithm to extract the surface temperature in the Malayer region and showed that the areas with water and vegetation had the lowest

temperature and played a significant role in reducing the temperature of the region. Bunai et al. (2020) compared two separate window and mono-window algorithms in Indonesia. The purpose of their research was to investigate the performance of these two algorithms in identifying the spatial distribution of the Land Surface Temperature using the mean square root of errors. Finally, the separate window method was introduced as an accurate method. Subhanil et al. (2020) estimated the Land Surface Temperature of Raipur City in India. They investigated their relationship with the normalized difference vegetation index and the normalized difference water index, emphasizing the urban heat island. Tewabe et al. (2020) identified Land Use changes in the Tana basin using remote sensing data, and satellite images. They found that in the Tana basin, agricultural land and residential areas increased by 15.61% and 8.05%, respectively. Using Landsat TM/ETM images from 1997 and 2013, Yusuf et al. (2020) investigated Land Use and land cover change in the Kuala Lumpur metropolitan area and found that high temperatures were more concentrated in built-up areas. Surface energy balance (SEB) models and remote sensing (RS) techniques were used to estimate ET in Todia Agricultural Farm (TAF) located in Riyadh Province, Kingdom of Saudi Arabia (Elkatoury et al., 2020)

Imran et al. (2022), by using remote sensing, assessed Land Use and land cover changes in summer and winter LST in Chittagong City (Bangladesh) between 1993 and 2020. Abdullah and Barua (2022) investigated the correlation between land cover characteristics and Land Surface Temperature (LST) in Chittagong Metropolitan Area (CMA) and used a single window algorithm (MWA) to estimate LST. Sajjad & Shankar (2023) assessed Land Use/ land cover change and its impact on LST using the RS technique in Khanwal district, Punjab (Pakistan) and showed that the decrease of NDVI and increase of LST has led to the decrease of greenness in that area. Other researchers, such as Ahmed et al., 2013; Chaudhuri and Mishra 2016; Bokaie et al., 2016; Sahana et al., 2016; De Jesus and Santana 2017; Ghosh et al., 2019; Tafesse & Suryabhagavan, 2019; Al Kafy et al., 2020; Akter et al., 2021 and Agbelade et al., 2023 evaluated the characteristics of land cover, Land Surface Temperature, and Land Use and used remote sensing technology in their studies.

In this research, taking into account the growth of Tabriz metropolis in terms of population, industry, and the importance of knowing about characteristics such as temperature and the necessity of knowing its spatial and temporal distribution, the spatial distribution of temperature in Tabriz County is estimated. The purpose of this research is to estimate the temperature of the Land Surface Temperature using single-channel, separate window, and Sebal algorithms and compare the temperature obtained from these three algorithms with different Land Uses in the study area. Comparing the temperature obtained from the mentioned algorithms with the data of the Tabriz station is one of the other aims of this research.

Materials and methods

Tabriz County, with an area of approximately 1781 square kilometers, is located in the center of East Azarbaijan province (Iran). The center of this County is Tabriz city. Tabriz County consists of two mountainous and plain regions. The approximate height of this County varies from 1300 to 2100 meters above sea level. This County is surrounded by the Sahand mountain range from the north and the Ainali mountain range from the south (Figure 1).

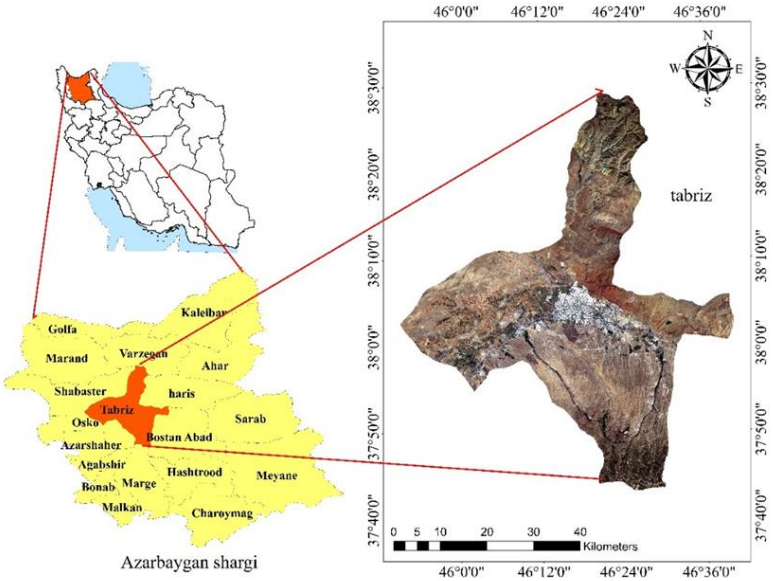

Figure 1. The geographic location of the Tabriz County

The data used in this research to extract the Land Use map and Land Surface Temperature includes the image of the OLI sensor and TIRS sensor of Landsat 8 satellite for 2019 pass 168 and rows 34 and 33. Due to the high radiation power of the sun and the absence of clouds, this image was taken from the hottest month of the year. The data from Tabriz's station at two centimeters above the land was used to verify the results. Specifications of OLI sensor bands, Landsat 8 are shown in Table 1.

Table 1. Specifications of OLI sensor bands, Landsat 8[1]

Bands	Resolution	Wavelength (Micrometer)
Band 1- Beyond Blue	30	0.435-0.451
Band 2- Blue	30	0.452-0.512
Band 3- green	30	0.533-0.590
Band 4- red	30	0.636-0.673
Band 5- Infrared close	30	0.851-0.879
Band 6- Infrared shortwave1	30	1.566-1.651
Band 7- Infrared shortwave2	30	2.107-2.294
Band 10- Thermal infrared1	100	10.60-11.19
Band 11- Thermal infrared1	100	11.50-12.51

After ensuring the absence of common errors, the obtained images were cut according to the studied area in ENVI 5.3 software. Then, by calculating the amount of radiance and applying the FLAASH method (Fast Line-of-Sight Atmospheric Analysis of Hypercubes), atmospheric corrections were made on them and algorithms for extracting the Land Surface Temperature were applied on them. Due to the high accuracy of the object-oriented

1- https://www.usgs.gov/faqs/what-are-band-designations-landsat-satellites

classification method, this method was used for classification, and the validation of the classification results was done in ENVI software using the obtained samples. In the segmentation, the multi-resolution method with different scales was used, considering the scale size of 2, the softness shape criterion equal to 0.4, and the Compactness parameter equal to 0.6. Figure 2 shows a part of the segmentation of the studied area.

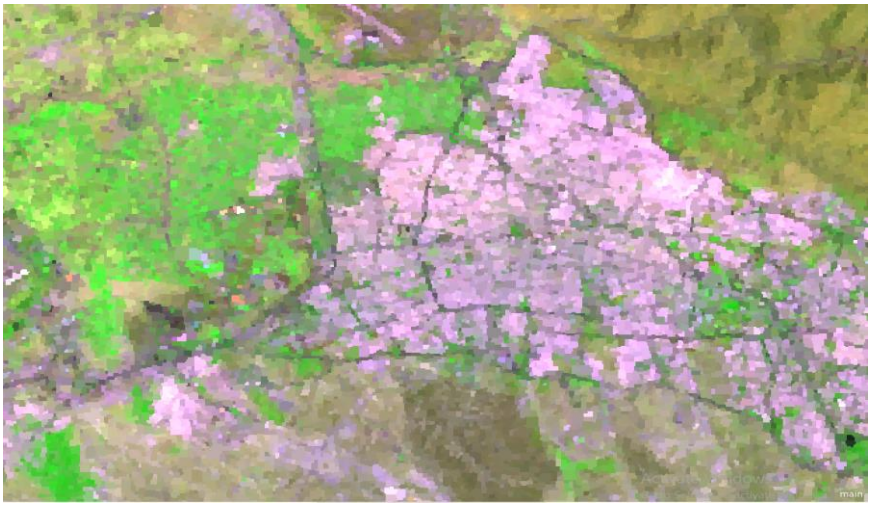

Figure 2. Part of segmentation with scale 2, Softness shape 0.4, and Compactness parameter 0.6 for the Tabriz County

The object-oriented classification method was used to classify Land Use into seven classes: dry pasture, residential, communication lines, cultivated and uncultivated agricultural land, industrial, and vegetation for 2019. The Normalized Difference Vegetation Index (NDVI) was obtained by equation 1 to express vegetation density information:

$$NDVI=(\frac{NIR-RED}{NIR+RED}) \quad (1)$$

In equation 1, NIR is the reflectance value in the near-infrared band, and RED is the reflectance value in the red band. The range of the NDVI index is between 1 and -1, and high values of this index indicate an increase in vegetation cover. The values for water and clouds are usually less than zero because, in this case, the reflectance of visible radiation is increased relative to the near-infrared reflectance. The standard range for bare soil and dense vegetation is 0.2 and 0.9, respectively (Asghari Saraskanroud et al., 2019). Estimates of emissivity using NDVI threshold values are shown in Table 2.

Table 2. Estimates of emissivity using NDVI threshold values (Ebrahimi Heravi et al., 2015)

Values	Constant and calculated coefficients
NDVI<-0.185	0.995
-0.185≤ NDVI ≤ 0.157	0.97
0.157≤ NDVI ≤ 0.727	IN (NDVI) 0.047 + 1.0094
0.727<NDVI	0.99

Equations 2 to 7 show the temperature extraction with the improved single-channel method. In these equations, LST: Land Surface Temperature, γ: gamma, ε: emissivity, T_{sensor}: thermal radiance, δ: delta, C_1 and C_2, Planck's radiation constant coefficients, $L_{sensor\lambda}$: thermal sensor radiance band 10 of TIRS and band 6 of TM, T_{sensor}: sensor brightness temperature, λ: wavelength of thermal bands 10 and 6, ψ_1, ψ_2 and ،ψ_3 indicates atmospheric correction parameters (Isaya Ndossi and Avdan 2016)

$$LST = \gamma[\varepsilon^{-1}(\psi_1 L_{sensor} + \psi_2) + \psi_3] + \delta \quad (2)$$

$$\gamma = \left\{\frac{c_2 L_{sensor.\lambda}}{T_{sensor}^2}\left[\frac{\lambda^4}{c_1} L_{sensor\lambda} + \lambda^{-1}\right]\right\}^{-1} \quad (3)$$

$$\delta = -\gamma\, L_{sensor.\lambda} + T_{sensor} \quad (4)$$

$$\psi_{1(\omega.T_a)} \equiv \frac{1}{\tau_{(\omega.T_a)'}} \quad (5)$$

$$\psi_{2(\omega.T_a)} \equiv -L^{\downarrow}_{atm(\omega.T_a)} - \frac{L^{\uparrow}_{atm(\omega.T_a)}}{\tau_{(\omega.T_a)'}} \quad (6)$$

$$\psi_{3(\omega.T_a)} \equiv -L^{\downarrow}_{atm(\omega.T_a)} \quad (7)$$

MODTRAN web platform has been used to estimate and simulate the atmospheric thickness and upward and downward atmospheric radiations for band 10 of Landsat 8 and band 6 of Landsat satellites. The mathematical structure for calculating LST with the separate window algorithm is as equation 8 (Rongali et al., 2018).

LST=TB10+C1 (TB10−TB11) +C2 (TB10−TB11)2 +C0 + (C3+C4W) (1−m) + (C5+C6W) Δm (8)

Where TB_{10}-TB_{11}: is brightness temperature, C: is algorithm coefficients, W: is the amount of water vapor in the atmosphere, and mΔ: is LSE difference (Feizizadeh et al., 2016). Constant and calculated coefficients used in the Split window algorithm are shown in Table 3.

Table 3. The values of the coefficients used in the Split window algorithm

Values	Constant and calculated coefficients
C_0	-0.268
C_1	1.378
C_2	0.183
C_3	54.3
C_4	2.238-
C_5	192.2
C_6	16.4

Atmospheric water vapor was obtained from equation 9.

$W_i = 0.0981*\{10*0.6108*\exp[\frac{17.27*(T0-273.15)}{237.15+(T0-273.15)}]*RH\} + 0.1679$ (9)

In this equation, W_i: is the amount of water vapor in the atmosphere, T_0: Land Surface Temperature (Kelvin), and RH: relative humidity. Estimating the emissivity on the ground surface was calculated separately in both thermal bands of the Landsat 8 satellite (Equation 10) (Valizadeh Kamran et al., 2017).

$LSE = Es\,(1-FVC) + Ev*FVC$ (10)

-۴

In this equation, LSE: is ground surface emissivity, E_S, E_v: is plant and soil emission for thermal bands according to Table 4, and FVC is the ratio of plant cover. The emissivity of plants and soil were shown in Table 4.

Table 4. The emissivity of plants and soil (Valizadeh Kamran et al., 2017)

Emissivity	B10	B11
Es	0.971	0.977
Ev	0.987	0.989

After calculating the emissivity of the earth's surface for each of the thermal bands, the difference and the average of these two bands were calculated based on equation 11 (Valizadeh Kamran et al., 2017).

$Mean\ E = (E^{10} - E^{11}) / 2$
(11)

Then the Emissivity difference between bands 10 and 11 was calculated from equation 12:

$\Delta m = LSE10 - LSE11$
(12)

The surface reflectance is the ratio of Reflected Radiant Energy to the incident spectral flux and is obtained by equation 13 (Entezari et al., 2016).

$$P_\lambda = \frac{\pi L_\lambda}{ESUN_\lambda . COS6 . d_r} \quad (13)$$

In equation 13, p_λ is the hemispheric spectral reflectance for each band, and $ESUN_\lambda$ is the average incident solar radiation above the atmosphere for each band with units of $W/m^2/sr/\mu m$. Albedo is the ratio of electromagnetic radiation reflected from the surface of the soil and plants to the sunlight incident on that surface and is obtained by equation 14 (Hatefi Ardakani and Rezaei Moghaddam, 2015).

$$\alpha = \frac{\alpha_{toa} - \alpha_{path-radiance}}{t_{sw}^2 2} \quad (14)$$

In equation 14, α_{toa} is the upper atmospheric albedo, $\alpha_{path\text{-}radiance}$ is the albedo due to the path radiance, and t_{sw} is the atmospheric transmittance. $\alpha_{path\text{-}radiance}$ is the average fraction of incident solar radiance for all bands scattered toward the sensor before reaching the earth's surface. The $\alpha_{path\text{-}radiance}$ values are between 0.025 and 0.045, considered 0.03 in the Sebal model. Corrected thermal radiance is the actual radiance emitted by the surface, corrected for atmospheric effects. Equation 15 was used to correct the thermal radiation emitted from the surface.

$$R_C = \frac{L_{NB} - R_P}{T_{NB}} - (1 - \varepsilon_{NB})\, Rsky \quad (15)$$

In equation 15, L_{NB} is the thermal band radiance, and T_{NB} is the atmospheric transmission capability in the thermal band.

Results & Discussion

To monitor the Land Surface Temperature and investigate the temperatures of different Land Uses and compare the algorithms for calculating the Land Surface Temperature, first, the Land Use map classes, including vegetation, dry pasture, communication lines, residential area, industrial areas, uncultivated agricultural land, and farmland was prepared. Then, the Land Use map was drawn in an object-oriented way.

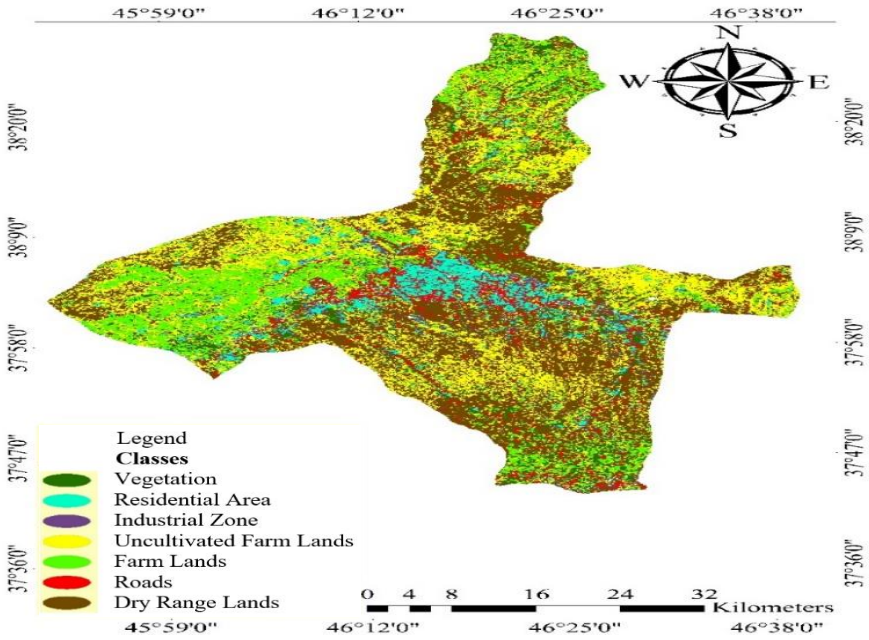

Figure 3. Land Use classification map of the Tabriz County

Using any kind of thematic information requires knowledge of its accuracy and correctness. The results of the classification validation performed in ENVI software showed an overall accuracy rate of 91% and a Kappa coefficient of 85%. The results of the assessment of the accuracy of the classification map by Land Use are presented in Table 5.

Table 5. Validation of classification results by object-oriented method for the Tabriz County

Land Use	Producer accuracy	User accuracy
Dry pasture	89.51	99.74
Vegetation	96.45	93.74
Farm	91.70	77.41
Uncultivated Farm	96.19	38.5
Industrial Zone	94.31	88.74
Residential Area	93.54	97.55
Lines of Communication	93.89	76.68
Overall Accuracy		91%
Kaya Coefficient		85%

After verifying the accuracy of the classification map, the temperature map of Tabriz County was prepared with Sebal, improved single channel, and separate window algorithms. The minimum and maximum temperatures in Tabriz County were obtained using Sebal's algorithm 12 and 51, separate windows 0 and 65, and improved single channel 0 and 50, respectively. Figures 4, 5, and 6 show the temperature map extracted from three algorithms with minimum and maximum temperatures.

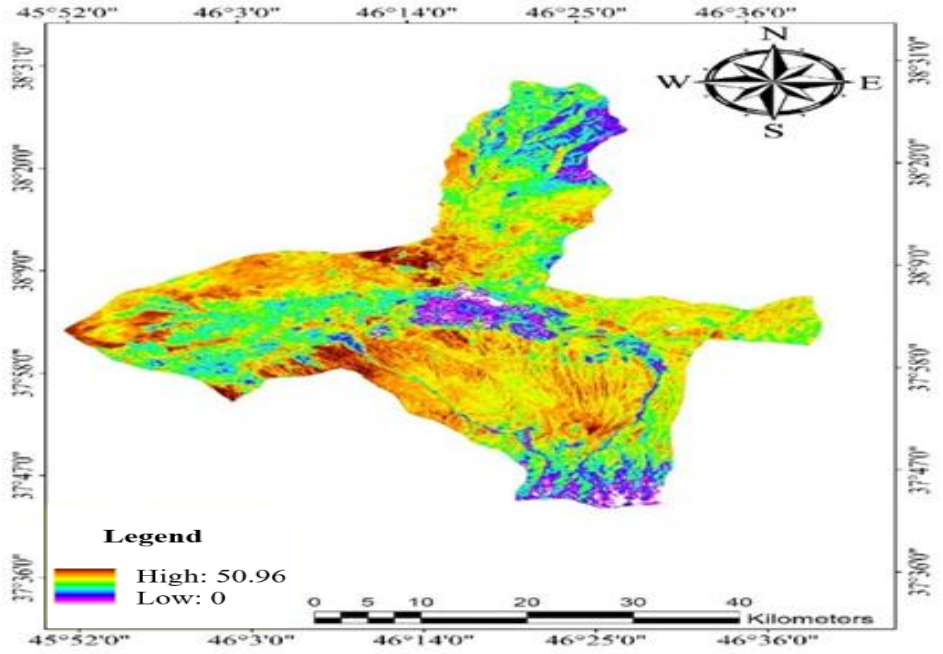

Figure 4. Land Surface Temperature map (c) with improved single-channel algorithm for the Tabriz County

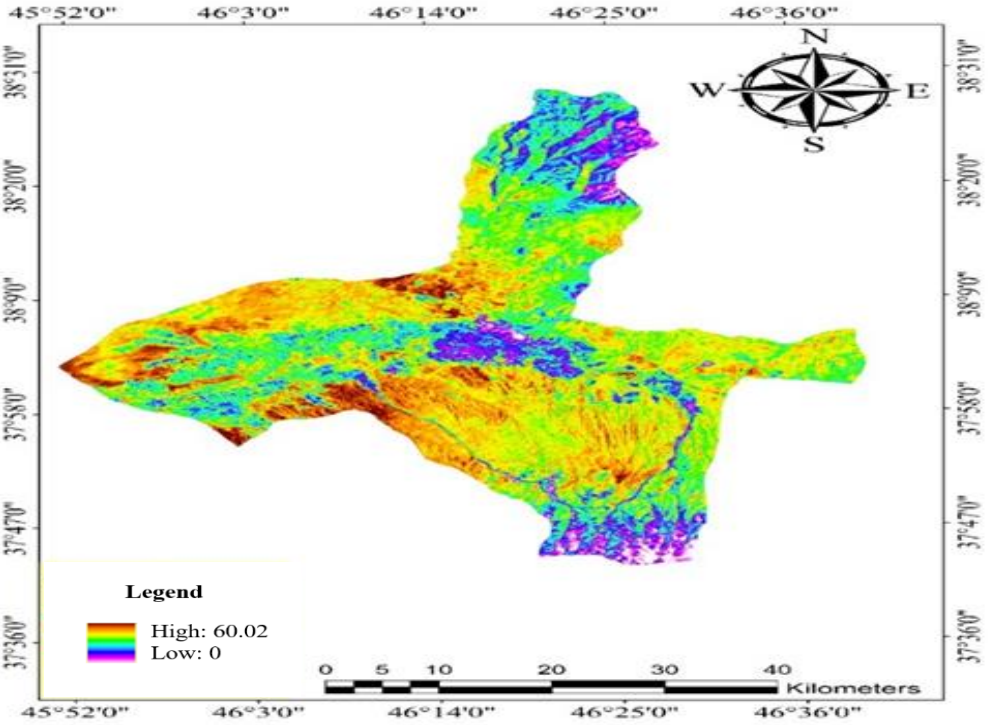

Figure 5. Land Surface Temperature (c) map with Split window algorithm for the Tabriz County

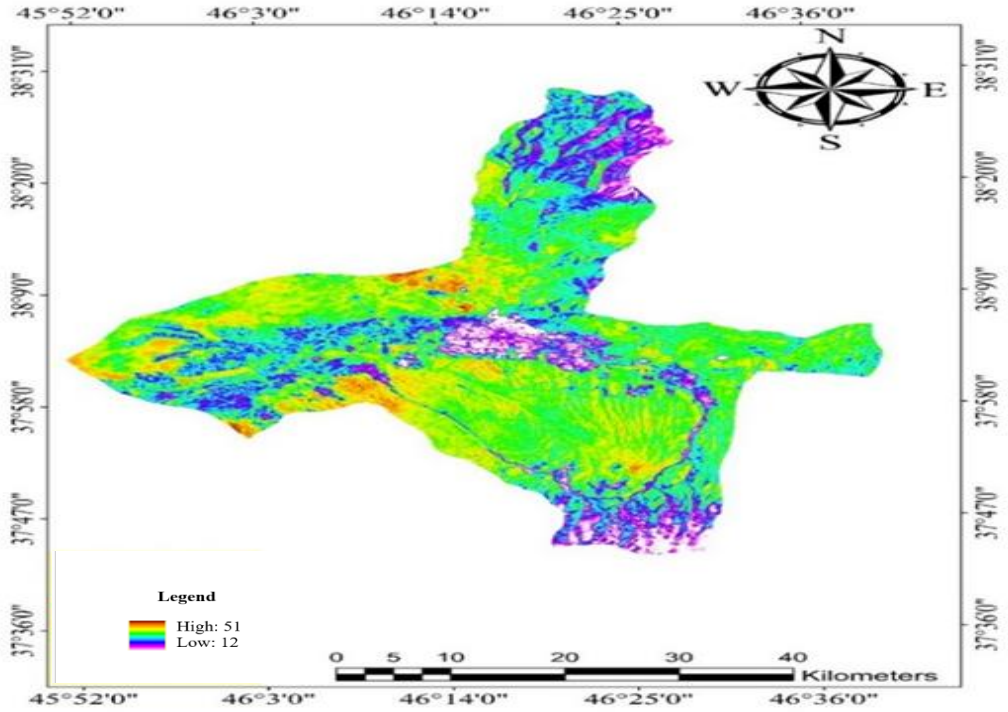

Figure 6. Land Surface Temperature (c) map with Sebal algorithm for the Tabriz County

The relationship between Land Use and surface temperature

Temperatures of different Land Uses were compared with each other in ArcGIS software. Comparison results showed that in all three investigated algorithms, the highest temperature in Tabriz County is related to the dry pasture area, and the lowest temperature is related to vegetation. In Tables 6, 7, and 8, the temperature of different Land Uses is presented. The obtained temperatures show the role and importance of vegetation in adjusting the temperature in the studied area. Comparing the temperatures obtained from the studied algorithms with the temperature of the Tabriz station showed a temperature difference of 5 degrees Celsius for the Sebal method, 6 degrees Celsius for the separate window method, and 4 degrees Celsius for the improved single channel method and this shows that the temperatures obtained from the improved single-channel method algorithm are the closest to the ground station temperature.

Table 6. Statistical characteristics of Land use with Split window algorithm for the Tabriz County

Classes	Average Temperature (c)	Standard Deviation
Dry Range Lands	**46**	4.616
Roads	40	7.061
Farm Lands	42	5.495
Uncultivated Farm Lands	46	4.611
Industrial Zone	42	6.197
Residential Area	40	6.56
Vegetation	**34**	8.708

Table 7. Statistical characteristics of Land use with Sebal algorithm for the Tabriz County

Classes	Average Temperature (c)	Standard Deviation
Dry Range Lands	**40**	3.240
Roads	35	4.680
Farm Lands	37	3.559
Uncultivated Farm Lands	39	3.193
Industrial Zone	36	4.925
Residential Area	34	5.877
Vegetation	**31**	3.352

Table 8. Statistical characteristics of Land use with an improved single channel for the Tabriz County

Classes	Average Temperature (c)	Standard Deviation
Dry Range Lands	**40**	3.27
Roads	35	5.664
Farm Lands	36	4.085
Uncultivated Farm Lands	39	3.200
Industrial Zone	36	5.876
Residential Area	34	6.133
Vegetation	**31**	7.612

The relationship between LST and NDVI

Vegetation is the major factor in the energy transfer between the biosphere and the atmosphere under the influence of vegetation. Vegetation is a vital factor in the energy transfer between the biosphere and the atmosphere, which has different effects on the meteorological elements of the surrounding areas. Vegetation is effective in climate processes such as energy transfer through air temperature, relative humidity, precipitation, radiation, and cloud cover. It is considered one of the important factors in the variability of the earth's climate. Due to the importance of the role of vegetation in the temperature of the earth's surface, the map of the vegetation of the studied area was also extracted in order to obtain a better understanding of the relationship between the vegetation and the Land Surface Temperature. Figure 7 shows the normalized differential vegetation index map for Tabriz

County. According to this figure, the minimum and maximum value of NDVI is -0.78 and 1, respectively. A comparison of Figure 7 with Figures 4 to 6 showed that areas without vegetation have higher surface temperatures than areas with vegetation. According to Figure 7, the northern and southern parts of Tabriz County have higher NDVI values than the central and eastern parts of this County. Since vegetation is one of the vital factors in the climate variability of the study area and plays an essential role in the interactions between surface processes, surface albedo, and surface temperature, environmental planners must pay special attention to increasing the NDVI value in the central and eastern regions of Tabriz County.

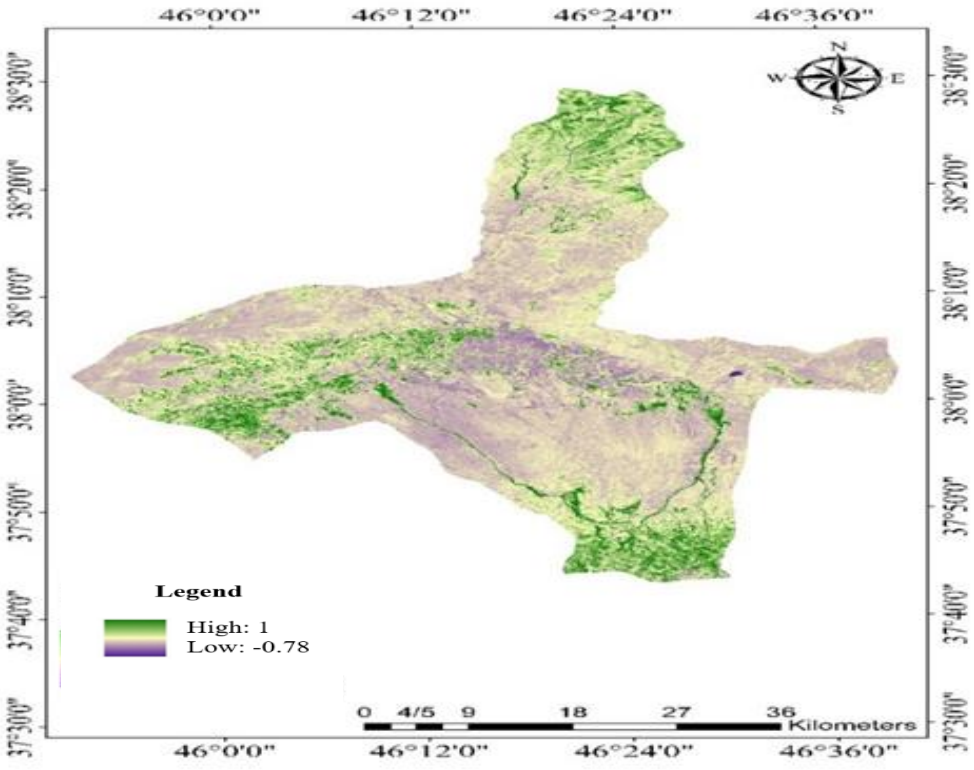

Figure 7. Normalized differential vegetation index map of the Tabriz County

Conclusion

The results of this research and other research showed that thermal remote sensing technology plays a vital role in measuring the Land Surface Temperature. In this regard, knowledge of different Land Uses and their relationship with Land Surface Temperature has a significant role in urban, environmental, and industrial planning. One of the most essential components in examining the Land Surface Temperature is Land Use, which determines the factors affecting the environment and human life. In this research, Sebal, single channel, and separate window algorithms were used. The result obtained from the Land Use classification of Tabriz County in July 2019 showed 90% accuracy and 89% kappa coefficient. After implementing the desired algorithms, the minimum and maximum temperatures for

vegetation and barren use were obtained for the Sebal algorithm 12 and 51, for the separate window 0 and 65, and for the improved single channel 0 and 50 degrees Celsius.
To prove the accuracy of the algorithms, the obtained temperatures were compared with the temperature of the Tabriz station (with minimum and maximum temperatures of 16 and 33 degrees Celsius). The temperature difference for Sebal, separate window, and improved single-channel methods was 5, 6, and 4°C, respectively, which shows that the temperature obtained with the improved single-channel method is the closest to the ground station temperature. This result is consistent with the findings of Asghari Saraskanroud et al. (2019) and Naseri (2020). The obtained temperatures show the role and importance of vegetation for the region and temperature adjustment. The improved single-channel method in measuring Land Surface Temperature on Landsat 8 images has high accuracy and is more consistent with the data of the station of Tabriz. This finding is also in line with the research results of Cristóbal et al. (2018). This research can be used in other fields, such as hot spot extraction. In order to obtain higher accuracy in Land Surface Temperature estimation, it is necessary to accurately measure the temperatures of different uses during the passage of the satellite using calibrated thermometers in the laboratory and compare the results with the extracted data.

References

Abdullah, S., and Barua, D. (2022) Modeling Land Surface Temperature with a Mono-Window Algorithm to Estimate Urban Heat Island Intensity in an Expanding Urban Area. Environ. Process 9, 14. https://doi.org/10.1007/s40710-021-00554-8

Agbelade, A.D., Akinyemi, T.C., and Ojerinde, G.E. (2023) Modeling and assessing the variation of land surface temperature as determinants to normalized difference vegetation index and land cover changes in Nigerian cities. Model. Earth Syst. Environ. https://doi.org/10.1007/s40808-023-01739-w

Ahmed, B., Kamruzzaman, M.D., Zhu, X., Rahman, M., and Choi, K. (2013) Simulating land cover changes and their impacts on Land Surface Temperature in Dhaka, Bangladesh. Remote Sens 5: pp 5969–5998. https://doi.org/10.3390/rs5115969

Akter, T., Gazi, M.Y., and Mia, M.B. (2021) Assessment of Land Cover Dynamics, Land Surface Temperature, and Heat Island Growth in Northwestern Bangladesh Using Satellite Imagery. Environ. Process 8: pp 661–690. https://doi.org/10.1007/s40710-020-00491-y

Al Kafy, A., Rahman, M.S., Faisal, A-A., Hasan, M.M., and Islam, M. (2020) Modelling future Land Use land cover changes and their impacts on Land Surface Temperatures in Rajshahi, Bangladesh. Remote Sens Appl Soc Environ 18:100314. https://doi.org/10.1016/j.rsase.2020.100314

Allen, R., Tasumi, M., Trezza, R., and Wim, B. (2002) SEBAL: Surface Energy Balance Algorithms for Land, Version 1.0, Funded by a NASA EOSDIS/Synergy Grant from the Raytheon Company through The Idaho Department of Water Resources.

Ang Kean, H., and Owi, W.P. (2018) The influence of land-use/land-cover changes on Land Surface Temperature: a case study of Kuala Lumpur metropolitan city, European Journal of Remote Sensing 51: 1, pp 1049-1069, DOI: 10.1080/22797254.2018.1542976

Asghari saraskanroud, S., Faal Naziri, M., and Ghale, E. (2019). The Relationship of Different Land Uses with Land Surface Temperature based on Spatial Correlation

(Moran) Analysis Using Landsat 8 Satellite Images (OLI) (Case Study: Ardebil City). Geography and Environmental Planning 30(1): pp 93-110. doi: 10.22108/gep.2019.117845.1170

Babalola, O.S., Akinsanola, A.A. (2016) Change Detection in Land Surface Temperature and Land Use Land Cover over Lagos Metropolis, Nigeria. J Remote Sensing & GIS 5: 171. doi:10.4172/2469-4134.1000171

Bokaie, M., Zarkesh, M.K., Arasteh, P.D., and Hosseini, A. (2016) Assessment of urban heat island based on the relationship between Land Surface Temperature and Land Use/land cover in Tehran. Sustain Cities Soc 23: pp 94–104. https://doi.org/10.1016/j.scs.2016.03.009.

Bunai, T., Rokhmatuloh, R., Wibowo, A., and Shidiq, I.P.A. (2020) Comparison Spatial Pattern of Land Surface Temperature with Mono Window Algorithm and Split Window Algorithm: A Case Study in South Tangerang, Indonesia, Earth and Environmental Science 149: pp 6. DOI 10.1088/1755-1315/149/1/012066.

Chaudhuri, G., and Mishra, N.B. (2016) Spatio-temporal dynamics of land cover and Land Surface Temperature in Ganges-Brahmaputra delta: a comparative analysis between India and Bangladesh. Appl Geogr 68: pp 68–83. https://doi.org/10.1016/j.apgeog.2016.01.002.

Cristóbal, J., Jiménez-Muñoz, J.C., Prakash, A., Mattar, C., Skoković, D., and Sobrino, J.A. (2018) An Improved Single-Channel Method to Retrieve Land Surface Temperature from the Landsat-8 Thermal Band. Remote Sensing 10(3): pp 431. https://doi.org/10.3390/rs10030431.

De Jesus, J.B., Santana, I.D. (2017) Estimation of Land Surface Temperature in Caatinga area using Landsat 8 data. J Hyperspectral Remote Sens 7(3): pp 150–157. https://doi.org/10.29150/jhrs.v7.3.p150-157

Dires, T., and Temesgen, F.,| Fei, L. (2020) Assessing Land Use and land cover change detection using remote sensing in the Lake Tana Basin, Northwest Ethiopia, Cogent Environmental Science 6: pp1, DOI: 10.1080/23311843.2020.1778998.

Ebrahimi Heravi, B., Rangzan, K., Riahi Bakhtiari, H., and Taghizadeh, A. (2015) Determination of urban surface temperature using landSat images (Case study: Karaj). *Journal of RS and GIS for Natural Resources 6*(2): pp 19-32.

Elkatoury, A., and Alazba, A.A. Mossad A (2020) Estimating Evapotranspiration Using Coupled Remote Sensing and Three SEB Models in an Arid Region. Environ. Process.7: 109–133 (2020). https://doi.org/10.1007/s40710-019-00410-w.

Entezari, A., Amir Ahmadi, A., Aliabadi, K., Khosravian, M., and Ebrahimi, M. (2016) Monitoring Land Surface Temperature and Evaluating Change Detection Land Use (Case Study: Parishan Lake Basin). Hydrogeomorphology 3(8): pp 113-139.

Feizizadeh, B., Didehban, K., and Gholamnia, K. (2016). Extraction of Land Surface Temperature (lst) based on landsat satellite images and split window algorithm study area: mahabad catchment. Geographical data 25(98): pp 171-181. https://sid.ir/paper/253219/en.

Ghosh, S., Chatterjee, N.D., and Dinda, S. (2019) Relation between urban biophysical composition and dynamics of Land Surface Temperature in the Kolkata metropolitan area: a GIS and statistical based analysis for sustainable planning. Model Earth Syst Environ 5: pp 307–329. https://doi.org/10.1007/s40808-018-0535-9

Hatefi Aardakani, M., and Rezaei Moghaddam., M.H. (2015) application of satellite images and GIS in the feasibility of the use of solar energy for providing lighting systems (case study: Zanjan-Tabriz highway). Arid regions geographic studies 6(21): pp 105-124.. https://sid.ir/paper/190665/en.

Imran, H.M., Anwar, H., Mahaad Issa, S., Mohan Kumar, D., Md.Rabiul, I., Kalimur, R., and Mansour, A. (2022) Land Surface Temperature and human thermal comfort responses to Land Use dynamics in Chittagong city of Bangladesh, Geomatics, Natural Hazards and Risk 13: pp 1, 2283-2312, DOI: 10.1080/19475705.2022.2114384

Isaya Ndossi, M., and Avdan, U. (2016) Application of Open Source Coding Technologies in the Production of Land Surface Temperature (LST) Maps from Landsat: A PyQGIS Plugin. Remote Sensing 8(5): 413. https://doi.org/10.3390/rs8050413.

Naseri, S. (2020) Estimating the Land Surface Temperature using the Single Channel algorithm and examining the impact of Land Use on temperature changes (Case study: Malayer county). Journal of Environmental Science Studies 5(2): pp 2477-2482.

Rongali, G., Keshari, A.K., and Gosain, A.K. (2018) Split-Window Algorithm for Retrieval of Land Surface Temperature Using Landsat 8 Thermal Infrared Data. J geovis spat anal 2, 14 https://doi.org/10.1007/s41651-018-0021-y

Sahana, M., Ahmed, R., and Sajjad, H. (2016) Analyzing land surface temperature distribution in response to land use/land cover change using split window algorithm and spectral radiance model in Sundarban Biosphere Reserve, India. Model. Earth Syst. Environ. 2, 81. https://doi.org/10.1007/s40808-016-0135-5

Sajjad, H., and Shankar, K. (2023) Land Use/land cover changes and their impact on Land Surface Temperature using remote sensing technique in district Khanewal, Punjab Pakistan, Geology, Ecology, and Landscapes 7: 1, pp 46-58, DOI: 10.1080/24749508.2021.1923272.

Sekertekin, A., and Bonafoni, S. (2020) Land Surface Temperature Retrieval from Landsat 5, 7, and 8 over Rural Areas: Assessment of Different Retrieval Algorithms and Emissivity Models and Toolbox Implementation. Remote Sensing 12(2): 294. https://doi.org/10.3390/rs12020294

Subhanil, G., Himanshu, G., Neetu, G., and Anindita, D. (2020) Analytical study on the relationship between Land Surface Temperature and Land Use/land cover indices, Annals of GIS 26: 2, pp 201-216, DOI: 10.1080/19475683.2020.1754291.

Tafesse, B., and Suryabhagavan, K.V. (2019) Systematic modeling of impacts of land-use and land-cover changes on land surface temperature in Adama Zuria District, Ethiopia. Model. Earth Syst. Environ 5: 805–817. https://doi.org/10.1007/s40808-018-0567-1

Ünal, Y.S., Sonuç, C.Y., and Incecik, S. (2020) Investigating urban heat island intensity in Istanbul. Theor Appl Climatol 139: pp 175–190, https://doi.org/10.1007/s00704-019-02953-2

Valizadeh Kamran, K., Gholamnia, K., Eynali, G., and Moosavi, M. (2017) Estimation Land Surface Temperature and extract heat islands using split window algorithm and multivariate regression analysis (Case Study of Zanjan). The Urban Research and Planning Quarterly 8(30): pp 35-50.

Wang, X., and Prigent, C. (2020) Comparisons of Diurnal Variations of Land Surface Temperatures from Numerical Weather Prediction Analyses, Infrared Satellite Estimates

and In Situ Measurements. Remote Sensing 12(3): pp 583. https://doi.org/10.3390/rs12030583.

Yusuf, Y.A., Pradhan, B., and Idrees, M.O. (2014) Spatio-temporal Assessment of Urban Heat Island Effects in Kuala Lumpur Metropolitan City Using Landsat Images. J Indian Soc Remote Sens 42: pp 829–837. https://doi.org/10.1007/s12524-013-0342-8.